Check for updates

Nanotubes of pristine poly(3-hexylthiophene) with modulable conductive properties: the interplay between confinement-induced orientation and interfacial effects

Lucas Leveque,[a] Eric Drockenmuller, [ID][a] Imad Laktineh,[b] Pierre Alcouffe,[a] Laurent David, [ID][a] Guillaume Sudre [ID][a] and Anatoli Serghei [ID]*[a]

Here we investigate nanotubes of poly(3-hexylthiophene) (P3HT) prepared by solvent casting using highly ordered AAO (anodized aluminum oxide) membranes as templates. Upon varying the thickness of the nanotubes between 13 nm and 44 nm, a rise in conductivity by five orders of magnitude is observed. For 44 nm thick P3HT nanotubes, a conductivity value higher than in the bulk is reported. The mechanism of this enhancement effect is evidenced by X-ray scattering structural investigations revealing an orientation of the crystalline domains along the long axis of the nanopores. Nanoconfinement in nanopores could represent thus a powerful tool to modulate, within many orders of magnitude, the conductive properties of conjugated polymers and give rise to nanomaterials exhibiting better properties than in the bulk.

1. Introduction

In the recent years, the fabrication of nanostructures of semi-conducting polymers has received significant interest in the field of nanoscience and nanotechnology[1,2] due to their unique properties that emerge at the nanoscale. Specific phenomena arising at this scale, driven by interfacial interactions and orientation and ordering effects, can lead to enhancement in physical properties and open thus new perspectives to potential applications in flexible electronic devices, sensors, transistors, solar cells *etc.* Due to its excellent charge transport properties and ease of processing, poly(3-hexylthiophene) (P3HT) is one of the most extensively studied conjugated polymers, both in the bulk[3] and under confinement into nanometric films[4] and nanopores.[5] Among various fabrication methods, the "template-assisted" method has emerged as a promising approach for the fabrication of P3HT nanostructures, such as nanowires,[6] nanotubes[7] or nanopillars.[8] This method involves the use of prefabricated porous templates, such as aluminum oxide nanoporous membranes (AAO),[9] as a confinement matrix. AAO membranes, fabricated by a two-step electrochemical anodization process, offer a highly-ordered hexagonally-packed structure of identical, independent nanopores whose

diameter and length can be easily controlled by adjusting the anodization conditions:[10] the nature and the concentration of the acid solution used as electrolyte, the temperature, the applied voltage and the anodization time. Thus, the AAO membranes represent ideal templates to fabricate nanotubes and nanowires of well-defined shapes and sizes by inserting polymers into nanopores. These polymer nanostructures can be kept confined in the nanopores or released by dissolving the AAO membranes and their physical properties can be investigated using different experimental techniques.[11] Studies on conjugated polymers confined in thin films,[12,13] nanotubes[14] and nanowires[15] reveal changes in the crystallization process and orientation of the polymer chains leading to optical and electronic properties that significantly differ from the bulk. For P3HT nanowires of 250 nm diameter, for instance, Jaime Martín *et al.*[15] revealed an alignment of the π–π stacking parallel to the nanopores axis. They also showed that, for thinner nanowires of 60 nm diameter, the π–π stacking is oriented perpendicular to the nanopores axis, indicating thus a strong impact of the nanopore diameter. D. Pourjafari *et al.*[16] investigated short P3HT nanowires (*i.e.* nanorods) prepared by AAO template-assisted synthesis and reported a conductivity value almost three times higher than in dense P3HT films. This effect was attributed to a longer conjugation length, higher crystallinity and lower band gap. J. Byun *et al.*[14] investigated P3HT nanotubes prepared by solution wetting of AAO templates and reported a conductivity 10 times higher than in the bulk, due to aligned P3HT chains along the nanotube direction.

[a] University Claude Bernard Lyon1, Ingénierie des Matériaux Polymères, CNRS UMR 5223, Villeurbanne, France. E-mail: anatoli.serghei@univ-lyon1.fr

[b] University Claude Bernard Lyon1, Institut de Physique des 2 Infinis, CNRS UMR 5822, Villeurbanne, France

In thin P3HT films,[17] a decrease in the relative degree of crystallinity with the film thickness is reported from 100% at 110 nm to around 20% for 10 nm, due to confinement effects.

Obviously, a wealth of different phenomena take place at the nanoscale and their overlapping contributions are not always easy to separate, making the interpretation of the experimental results difficult and hindering a complete understanding of the impact of nanometric confinement on polymer properties. On one hand, as opposed to bulk, nanoconfinement implies a dramatically enhanced surface-to-volume ratio that is expected to boost surface-induced effects.[18] On the other hand, the geometric nanoconfinement due to nanopores diameter is also known to significantly impact polymer properties.[14,15,19] Moreover, molecular interactions between the polymer and the internal surfaces of the confining substrate can give rise to a specific molecular packing leading to the formation of adsorbed layers with strong impact on nanostructure properties and performance.[20] All these phenomena play an important role at the nanoscale but a clear approach to separate their overlapping contributions is not yet systematically discussed in scientific literature. Our study proposes an effective way to address this challenge by using two complementary approaches. On one hand, a systematic comparison between the conductive properties of P3HT in the bulk and confined in nanowires and nanotubes is conducted. To our best knowledge, this comparison between bulk, nanowires and nanotubes has not been yet studied in scientific literature so far. On the other hand, by systematically varying the nanotube thickness, a quantitative analysis of surface-induced effects will be carried out: with decreasing the nanotube thickness, sample regions closer to the nanopores surface will be explored. This will allow one to separate surface-effects, predominant for thinner nanotubes, from the impact of geometrical nanoconfinement that plays an important role for thicker polymer nanotubes and polymer nanowires. Detailed studies on conductive nanotubes of conjugated polymers as a function of nanotubes thickness have been not yet reported in scientific literature so far. Thus, our study contributes to a better understanding of confinement effects on the conductive properties of conjugated polymers, by a comprehensive comparison between bulk, nanowires and nanotubes combined with a systematic variation of the nanotube thickness. In addition, our results prove the possibility of broadly modulating the conductive properties of conjugated polymer nanotubes to reach conductivity values higher than in the bulk, which can be of significant importance in developing new functional nanomaterials with enhanced conductive properties.

2. Materials and methods

2.1 Materials

The AAO membranes used in this study as templates for nanostructures were provided by Topmembranes Technology. The diameter of the nanopores was 220 ± 2 nm, the thickness of the membrane was 52 ± 1 μm, and the porosity of the membrane was $22 \pm 1\%$. The dimensions of the AAO membranes and their uncertainties were determined directly from the images taken by electron microscopy presented in this work. P3HT was provided by 1-material (Dorval, Quebec, Canada), with a regioregularity RR = 90%,[21] a number average molar mass $M_n = 18$ kg mol^{-1} and a dispersity $Đ = 2.0$. Chloroform provided by Carlo Erba was used to dissolve P3HT.

2.2 Sample preparation

The P3HT nanotubes were fabricated by the "template wetting" method using AAO membranes (Fig. 1). A certain amount of P3HT was put in chloroform and then placed on a hot plate
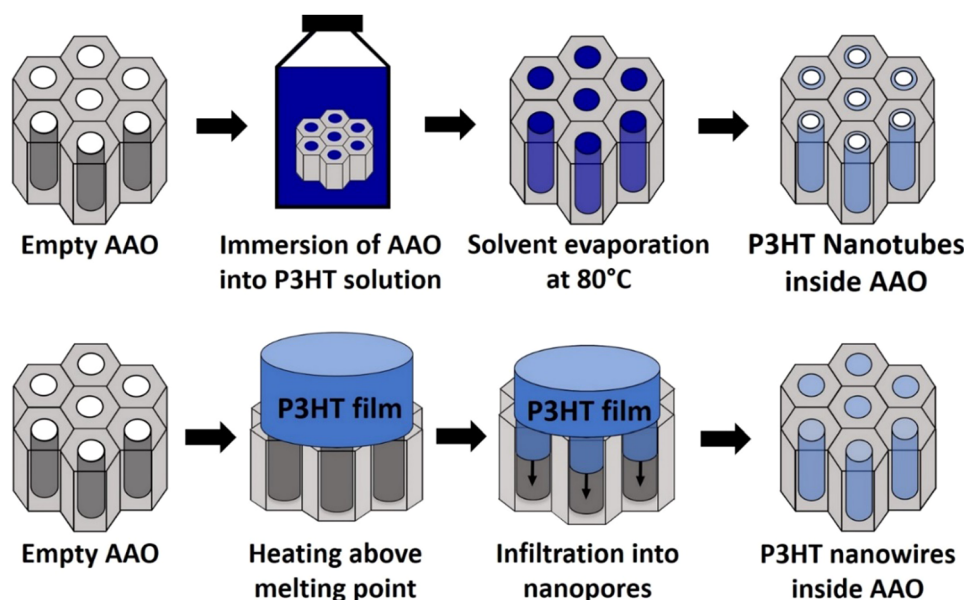

Fig. 1 Schematic representation of the preparation of polymer nanotubes (by solvent wetting, on the top) and polymer nanowires (by melt wetting, at the bottom), using AAO membranes as templates.

Table 1 List of the P3HT nanotube samples and their solutions used to produce them. The thickness of the nanotubes was determined by SEM and TEM measurements

Sample name	P3HT concentration (mg ml^{-1})	Volume percentage of P3HT (%)	Nanotubes thickness (nm)
NT1	100	7.9	44 ± 1
NT2	50	4.1	31 ± 1
NT3	25	2.1	23 ± 1
NT4	10	0.9	18 ± 1
NT5	5	0.4	13 ± 2

heated at 50 °C for 30 min to aid in the dissolution of the polymer in the solvent. Several concentrations were used in this study (see Table 1). The empty AAO membranes were first immersed in acetone and then chloroform for 1 h to eliminate any organic impurities. They were then cleaned with plasma to assure total purification and subsequently immersed in the P3HT/chloroform solution for 12 h to allow the polymer solution to infiltrate the nanopores. The AAO membranes were then removed from the solution and placed under a nitrogen atmosphere at 80 °C for 1 h to ensure the evaporation of the solvent contained in the nanopores. After solvent evaporation, the internal walls of nanopores were covered by P3HT, leading to the formation of nanotubes. The outer surfaces of the AAO membranes were subsequently cleaned using a cotton swab dipped in chloroform to remove any P3HT excess from the surface.

The P3HT nanowires were fabricated by "melting flow template" method using AAO membranes (Fig. 1). A P3HT film was made by drop-casting a P3HT/chloroform solution on a glass substrate. The sample was subsequently annealed and the resulting polymer film was then deposited on the surface of the AAO membrane, previously metallized with a 40 nm gold-layer. The system was then heated under nitrogen atmosphere and kept for 12 h at 250 °C (above the melting point of P3HT) to allow the polymer to infiltrate the nanopores (Fig. 1). The procedure of polymer infiltration into nanopores from the melt is described in ref. 22 and 23.

2.3 Methods

2.3.1 Electrical measurements. The electrical conductivity and the phase transitions of P3HT were measured using a novocontrol alpha broadband dielectric/impedance spectrometer (BDS) operating in the frequency range from 10^7 Hz to 10^{-3} Hz. The applied voltage amplitude was 0.1 V. The value of conductivity was determined by taking into account the DC-plateau observed in the low frequency range in the conductivity spectra of σ' measured by BDS. The P3HT nanowires and nanotubes were measured directly inside the AAO membranes (see Fig. S1 from SI). To ensure an optimal electrical contact between the electrodes and the sample, a 40 nm gold layer was deposited on both surfaces of the empty AAO membranes by sputtering, using a "Cressington Sputter Coater", prior to the preparation of nanotubes or nanowires. Bulk-type samples were measured in the form of 120 ± 3 μm thick films made by drop-casting directly from the same P3HT solution used to fabricate

the nanotubes. The value of conductivity of nanotubes and nanowires was calculated by taking into account the effective area of the polymer samples (S_{eff}), according to the eqn (1) and (2), respectively:

$$S_{eff} = S_t \times P \times e \qquad (1)$$

$$S_{eff} = S_t \times P \qquad (2)$$

where S_t represents the total surface area of the gold-sputtered electrodes, P the porosity, e volume fraction of nanopores occupied by the polymer and R the nanopore radius. Eqn (1) was used for nanotubes and eqn (2) for nanowires.

2.3.2 Morphological measurements. SEM measurements were carried out using a scanning electron microscope (SEM Zeiss Merlin compact). Empty AAO membranes were metallized with a thin layer of copper (10 nm) and directly observed by SEM microscope. AAO membranes containing the polymer nanostructures were immersed in liquid nitrogen during 30 s to rigidify the polymer structure followed by depositing a droplet of a 0.1 M NaOH solution on top of the samples to partially dissolve the aluminum oxide and reveal the nanostructures (see Fig. S2 from SI). Once partially released, the nanostructures were rinsed with deionized water and placed at 100 °C under nitrogen flow for 1 h to completely evaporate the water contained inside the nanotubes. The P3HT nanotubes were also investigated by transmission electron microscopy using a Jeol 1400Flash electron microscope. The AAO membranes containing P3HT nanotubes were immersed in a 0.1 M NaOH solution until complete dissolution, leading to an aqueous suspension of nanotubes. The suspension was poured inside a glass vial connected to a vacuum pump and then filtered using deionized water using a 100 nm Whatman filter to remove all impurities. After 5 cycles of filtration, TEM grids were deposited in the aqueous suspension at the bottom of the glass vial and the water was completely evaporated in order to deposit the nanotubes/nanowires onto the TEM grids for analysis. A thermal treatment of 1 h at 100 °C under nitrogen flow was subsequently applied to evaporate the remaining water. The TEM grids were then analyzed using a TEM microscope.

2.3.3 DSC measurements. DSC measurements were performed on bulk-type samples in the form of 120 μm P3HT films, using a DSC Q200 1854 from TA Instruments. Three cycles of cooling/heating were conducted under a nitrogen atmosphere with a flow rate of 50 mL min^{-1} and heating/cooling rate of 5 °C min^{-1}. The first cycle was performed to eliminate the thermal memory of the polymer, while the second and third cycles were carried out to measure the calorimetric response and ensure the reproducibility of the obtained results.

2.3.4 Structural measurements. WAXS measurements were performed at the European Synchrotron Radiation Facility (ESRF, Grenoble, France) on the BM2-D2AM beamline located in Grenoble, France. The scattering patterns of the samples including 120 μm thick P3HT films, nanotubes and nanowires were recorded with an incident photon energy of 18 keV, using a two-dimensional photon counting pixel detector (WOS ImXPad[24] placed at 27.7 cm from the sample). The two-dimensional data

were corrected by taking into account the flat field response of the detector. The signal of the empty cell was subtracted from the scattering images of all studied samples. The nanotubes and nanowires were measured inside the AAO membranes in transmission mode along the axis of the nanopores (on-plane configuration) with the scattering vector q perpendicular to the nanopore axis. Further data treatment involved the subtraction of the signal of the empty AAO membrane from the scattering images of the nanostructures (*i.e.* AAO filled with P3HT).

3. Results and discussion

The morphology of the P3HT nanowires and nanotubes prepared using AAO membranes in shown in Fig. 2, as measured by our SEM and TEM investigations. Further investigations by energy dispersive spectroscopy conducted on a cross-section of fractured AAO membranes containing the P3HT nanostructures confirmed polymer coverage along the entire length of the nanopores (Fig. S3 from SI).

The P3HT nanotubes present a very smooth and regular morphology (Fig. 2C and D). The quality of the nanostructures is due to the highly ordered and monodispersed morphology of the AAO nanopores used as template. Because their length is
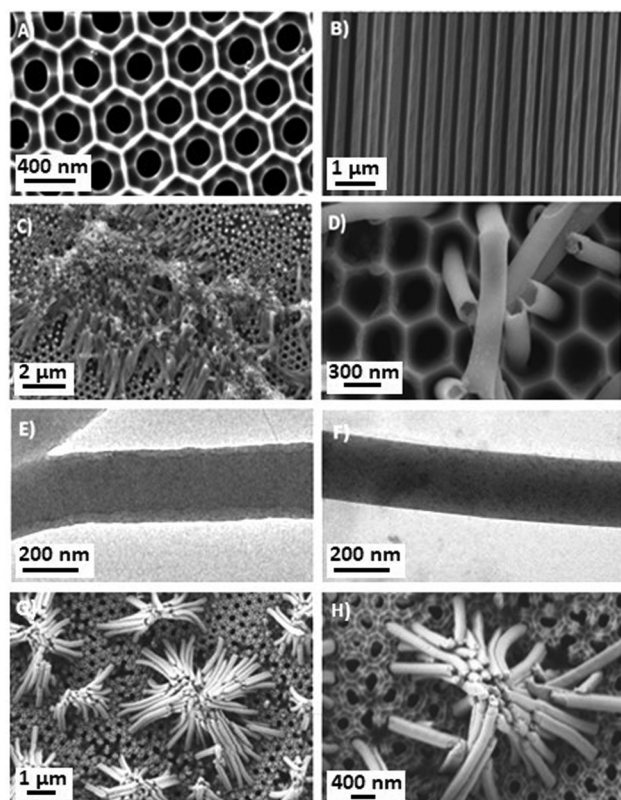

Fig. 2   (A) and (B) SEM images of empty AAO membranes showing highly ordered nanopores of well-defined shape and size. (C) and (D) SEM images of P3HT nanotubes, after a partial dissolution of the AAO membrane. (E) and (F) TEM images of P3HT nanotubes and nanowires after a complete dissolution of the AAO membrane. (G) and (H) SEM images of P3HT nanowires, after a partial dissolution of the AAO membrane.
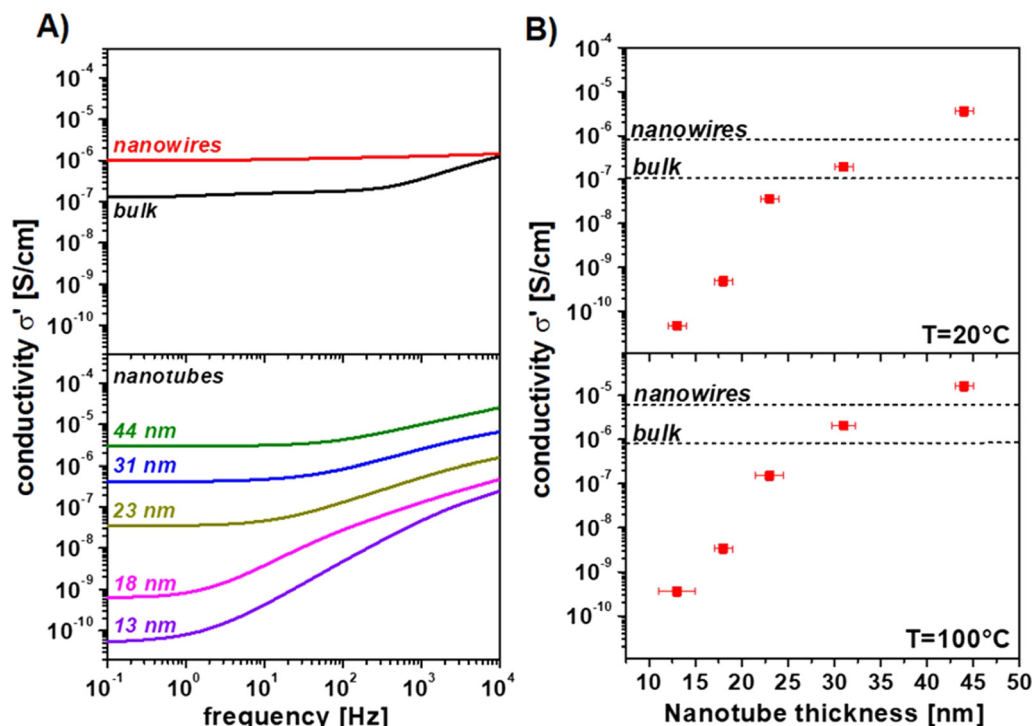
much larger than their diameter, the nanotubes collapse upon themselves after being partially released by dissolution of the AAO membranes. K. Smith *et al.* studied this phenomenon and quantified nanotube aggregation depending on the dissolution time of the AAO membrane.[25] P3HT nanowires show a similar behavior (Fig. 2G and H) after partial dissolution of the AAO membrane. The thickness of the nanotubes can be systematically varied from 13 to 44 nm by adjusting the concentration of the P3HT solution used for the fabrication (Table 1). Fig. 2E and F shows the TEM images of P3HT nanotubes and nanowires. The difference in contrast between the center and the surface of the P3HT nanostructures evidences the tubular morphology characteristic for nanotubes.

The electrical conductivity of the samples was measured by broadband dielectric spectroscopy (BDS) as a function of frequency for P3HT in three different forms: bulk, nanowires and nanotubes of various thicknesses (Fig. 3A). At high frequencies, an increase of conductivity with increasing frequency is observed, related to a capacitive behavior. The conductive regime, arising from a long-range diffusion of free charges, appears at low frequencies, where a plateau in conductivity is observed, corresponding to the DC-conductivity of the investigated nanostructures. This plateau value will be further considered as the value of the DC-conductivity in the analysis carried-out in the present study. As shown in Fig. S4 in SI, the conductivity of the empty AAO membranes is of the order of 10^{-14} S cm^{-1} at 20 °C, in good agreement with previous studies.[26] This value is by many orders of magnitude smaller than the conductivity of the P3HT nanostructures (typically above 5×10^{-11} S cm^{-1}), implying a negligible contribution of the empty AAO membrane to the measured electrical current.

Moisture absorption impacting the conductivity measurements of semiconducting polymers is a well-known phenomenon.[27,28] To prevent moisture effects and equilibrate the samples, a thermal treatment of at least 12 h (36 h for bulk samples) was performed at 100 °C under anhydrous nitrogen flow in the cryostat of the BDS measurement cell. The conductivity investigations were subsequently carried out without exposing the samples to ambient air again. The evolution of conductivity of bulk, nanowires and nanotubes upon thermal equilibration is shown in Fig. S5 in SI.

Extracted from Fig. 3A and B depicts the evolution of DC-conductivity as a function of nanotubes thickness at 20 °C and 100 °C. The trend of conductivity evolution with thickness remains the same at 100 °C and at 20 °C, only the intrinsic value of conductivity becomes overall higher at 100 °C than at 20 °C. This increase in conductivity with increasing temperature, due to an enhanced charge mobility, is well-documented in the scientific literature for conjugated polymers.[28–30]

From these conductivity measurements carried out between 20 °C and 100 °C, the activation energy for charge transport was calculated for each sample according to the Arrhenius relation:

$$\sigma(T) = \sigma_0 e^{\frac{-E_a}{k_B T}}$$

were σ_0 is constant, k_B is the Boltzmann constant, T the

Fig. 3 (A) Conductivity σ' at 20 °C of the bulk P3HT and P3HT nanowires (upper graph) and of P3HT nanotubes of different thicknesses, as indicated (lower graph), as a function of frequency. The plateaus observed at low frequencies correspond to the DC-conductivity value of the investigated materials. (B) DC-conductivity of P3HT nanotubes as a function of nanotubes thickness measured at 20 °C (upper graph) and 100 °C (lower graph), as indicated. The dotted lines correspond to the conductivity values of bulk P3HT and P3HT nanowires.

temperature and E_a the activation energy associated to the activation of the conductivity $\sigma(T)$.

A value of 290 ± 30 meV (or 27.98 ± 2.89 kJ mol^{-1}) was found for activation energy in the bulk, in good agreement to the values reported in the scientific literature (ref. 31 in the revised manuscript). For the nanotubes, a slightly lower activation energy was determined (222 ± 32 meV or 21.42 ± 3.09 kJ mol^{-1}), indicating that the nanoconfinement facilitates the charge transport mechanism by reducing the energy barrier associated with the thermally activated hopping process.

The dashed lines represent the DC-conductivity values of the P3HT nanowires and bulk. At 20 °C, the P3HT nanowires of 220 nm diameter exhibit a DC-conductivity value of $(7.7 \pm 2.2) \times 10^{-7}$ S cm^{-1}, thus 7 times higher than that of the bulk $(\sigma'_{bulk} = (1.1 \pm 0.3) \times 10^{-7}$ S cm$^{-1})$. A more pronounced conductivity enhancement effect is found for the P3HT nanotubes of 44 nm thickness which exibit a conductivity value of $(3.6 \pm 0.9) \times 10^{-6}$ S cm^{-1}, thus 14 times larger than in the bulk. Quite remarkably, the P3HT nanotubes of 44 nm thickness are more conductive than the P3HT nanowires, and both samples are more conductive than the bulk. A possible hypothesis to explain this enhancement effect can be related to a modification of the crystalline structure of the P3HT confined at the nanoscale. Additionally, orientation effects of the polymer chains inside the nanopores favoring the charge transport process along the nanopores axis could be considered as well. In the literature, previous studies have reported an enhanced conductivity in polymer nanowires[16] and nanotubes[14] compared to bulk and

this effect was attributed to an orientation of the polymer chains along the pore axis. However, a significant difference in conductivity between nanowires and nanotubes is revealed in our present study, suggesting a much more efficient orientation effects in nanotubes.

The evolution of conductivity of P3HT nanotubes shows a pronounced dependence, spanning over 5 orders of magnitude, upon varying the nanotubes thickness. The thicker the nanotubes, the higher the conductivity. The decrease in the conductivity with decreasing thickness can be explained by an adsorption of polymer chains in the nanometric vicinity of the nanopores walls. This phenomenon, known as "dead-layer", is well-documented in the scientific literature.[20] Within several nanometer from the surface (up to 6 nm),[32] polymers chains are packed differently than in the bulk, due to the impact of interfacial interactions. This leads to a dramatic slowing-down of the relaxation rate of polymer segments, impacting both the rotational and translational diffusion times. Both are known to be correlated in polymer materials,[33] with the last one being directly related to the value of conductivity according to the Einstein–Smoluchowski relationship written as:

$$\sigma_{DC} = nq\mu = \frac{nq^2\mu D}{k_B T} = \frac{nq^2\mu}{k_B T}\frac{\lambda^2}{2\tau_e} \tag{3}$$

Where with n is the charge density, q the elementary charge, μ the charge mobility, k_B the Boltzmann constant, T the temperature, D the diffusion coefficient, λ the hopping length of the charge carriers and τ_e the hopping time. This relationship can be

summarized as $\sigma_{DC} \approx \tau_e^{-1}$, known as the Barton–Nakajima–Namikawa (BNN) relationship.[33] In the nanometric vicinity of the nanopores walls, the hopping rate is thus expected to be dramatically slowed-down, leading consequently to a drastic decrease in conductivity. The thinner the nanotubes of P3HT, the larger the impact of the "dead-layer" on the conductivity of P3HT nanotubes. This effect has been also observed in ultra-thin films deposited onto SiO$_2$ substrates, showing a reduction of the charge mobility with decreasing the film thickness[17] because of the interaction between the polymers and the SiO$_2$ substrate.

The charge transport phenomenon in P3HT is known to strongly depend on the crystallization state.[34,35] In nanometric films, the crystallization state is expected to differ from the bulk, due to surface interactions and orientation and ordering effects. In the present study, the crystallization and melting temperature of P3HT in the bulk and confined in nanowires and nanotubes have been investigated by BDS. This method, based on measurements of permittivity as a function of temperature at different frequencies, has been proved highly efficient in studying the phases transitions of polymers confined at the nanoscale.[36] It relies on the proportionality relationship existent between the first derivative of permittivity and the first derivative of density, according to the Clausius–Mossotti relation:

$$\frac{\varepsilon' - 1}{\varepsilon' + 2} = \frac{N_a \alpha_{mol}}{3\varepsilon_0 M}\rho \tag{4}$$

where N_A is the Avogadro constant, α_{mol} the molecular polarizability, ε_0 the vacuum permittivity, M the molar mass, ε' the permittivity and ρ the density. The Clausisus–Mossotti relation implies thus:

$$\frac{\partial \varepsilon'}{\partial T} \approx \frac{\partial \rho}{\partial T} \tag{5}$$

which can be successfully used to characterize phase transitions of polymers and other materials, since phase transitions are generally accompanied by changes in density. This method has been used in the current study for the determination of the crystallization and melting temperatures of P3HT in the bulk and nanoconfined states. For the bulk, a P3HT sample in the form of a 120 μm thick film was measured by BDS and DSC under a nitrogen atmosphere following three cooling/heating cycles at 2 °C minute^{-1}. The first cycle was conducted to erase the thermal history of the samples, and the subsequent two cycles were carried out to characterize the phase transitions and ensure the reproducibility of the results. Fig. 4 compares the results obtained from the BDS and DSC experiments. During the cooling cycle, P3HT exhibits a shoulder at 220 °C followed by a clear crystallization peak at 208 °C, as shown by both techniques. During the heating cycle, P3HT shows a single melting peak at 232 °C in BDS and at 235 °C in DSC.
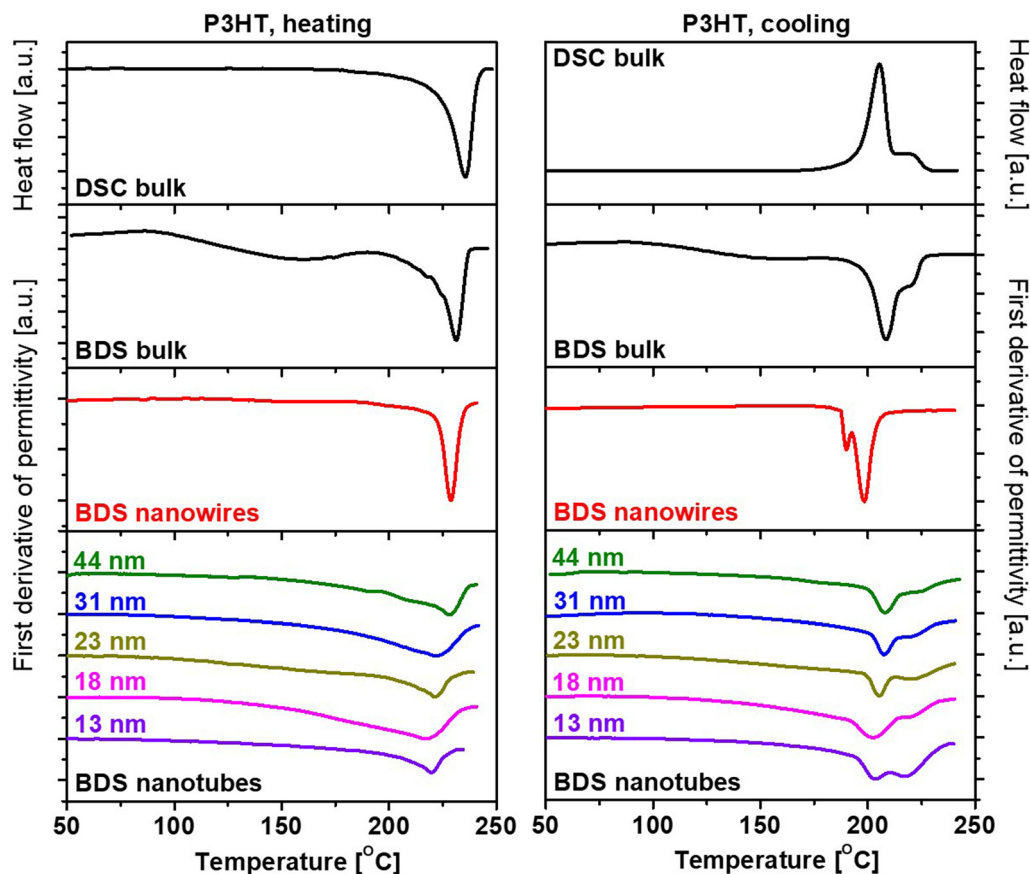

Fig. 4 Melting (left) and crystallization (right) of bulk P3HT, nanowires and nanotubes of different thicknesses, measured by DSC and BDS.

These results prove the good agreement between DSC and BDS in measuring polymer phase transitions. For nanotubes and nanowires, the material amount is too small to be measurable by DSC, but BDS has proven to be a highly efficient method for measuring extremely small amounts of matter.[37] This method was first applied to empty AAO membranes to demonstrate that no variations in permittivity appear over the investigated temperature range (Fig. S6 in the SI), indicating that the change phase transition peaks detected in the first derivative of permittivity (Fig. 4) can be directly attributed to the polymer confined into the nanopores. For the P3HT nanotubes during the cooling cycle, a distinct crystallization peak appears around 210 °C with a visible shoulder around 220 °C depending on the thickness of the nanotubes. The temperature of this crystallization peak decreases with decreasing the thickness of the nanotubes (see Table 2).

However, the temperature shifts between the bulk material and the nanotubes are rather small, and the shape of the crystallization peak remains the same for both systems. A similar behavior is observed during the heating cycle: one (asymmetrical) melting peak is detected for all nanotubes and the melting temperature decreases with decreasing the thickness of the nanotubes. This behavior is well-known in the case of thin polymer films.[38,39] From a geometrical point of view, polymer nanotubes can be assimilated to nanometric films folded upon themselves to form hollow cylinders, explaining the similar behavior observed for the crystallization and melting temperatures under conditions of nanoconfinement. For P3HT nanowires, during the heating cycle, the melting peak is similar to that of the bulk. However, the behavior during crystallization is different. Two crystallization peaks appear at 190 °C and 198 °C, which differ from both the bulk and nanotube samples. In fact, P3HT nanowires are morphologically different from nanotubes, since they cannot be assimilated to ultra-thin films. This indicates a different molecular arrangement upon crystallization between the nanowires and the nanotubes.

To understand the conduction properties of P3HT confined in nanopores, WAXS investigations were conducted in the present study to analyze the effects of confinement on the crystalline structure of the samples. The crystalline structure of bulk and thin P3HT films has been extensively studied in the scientific literature. P3HT is a semi-crystalline polymer with a crystalline structure arranged in a monoclinic lattice ($\alpha = \beta = 90°$, $\gamma = 87°$) with lattice parameters $a = 1.63$ nm, $b = 0.76$ nm, and $c = 0.77$ nm.[40] The crystallinity of P3HT varies depending on its molar mass,[41] its regioregularity,[42] its thickness[17] and

presents a long periods length of 1.1 nm.[43] In organic semiconductors, such as P3HT, charge transport is intrinsically linked to the molecular structure and the solid-state packing of the polymer chains.[44] The alternating single and double bonds along the polymer backbone create a conjugated system, which facilitates delocalization of π-electrons. This conjugation opens an energy gap, essential for semiconducting behavior. The efficiency of charge transport P3HT is strongly influenced by the arrangement of polymer chains in the solid state, where molecular packing plays a critical role in determining intermolecular electronic coupling.[45,46] P3HT exhibits an anisotropic charge transport behavior due to its semi-crystalline nature. This anisotropy is defined by three distinct axes: the lamellar stacking axis (a-axis), the π–π stacking axis (b-axis), and the axis along the conjugated backbone (c-axis).[46] Among these, the c-axis, aligned with the conjugated thiophene units, supports the highest charge mobility owing to the covalent linkage of the conjugated units, enabling efficient intra-chain charge transport.[46–48] In contrast, the a-axis, corresponding to lamellar stacking of the side chains, typically shows the slowest charge transport due to the weak electronic coupling between adjacent polymer layers. The b-axis, associated with π–π stacking between conjugated backbones, provides intermediate charge transport properties, with relatively faster inter-chain charge transfer due to the favorable orbital overlap between neighboring thiophene units.[46] Charge transport within P3HT films is further influenced by the balance between crystalline and amorphous regions and it requires percolated network of conjugation, usually through well-ordered polymer aggregates.[49] Theses aggregates, formed by well-ordered crystalline domains, play a pivotal role in facilitating charge transport, as they exhibit longer conjugation lengths and tighter π–π stacking compared to the disordered amorphous regions.[47] These crystalline regions serve as efficient pathways for charge carriers, while amorphous domains, characterized by disrupted chain planarity and reduced conjugation lengths, pose barriers to efficient charge transport.[49,50] The presence of torsional defects in these disordered regions leads to charge trapping and necessitates interchain hopping, a process significantly slower than transport along a single conjugated chain, leading to an overall reduction of charge mobility in amorphous regions with values limited to approximately 0.1 cm^2 V^{-1} s^{-1}, thus, several orders of magnitude lower than in crystalline regions.[47,49,51] Additionally, the difference in energy gaps between crystalline and amorphous regions exacerbates the charge transport limitations in semi-crystalline films. Shorter conjugation lengths in amorphous regions lead to higher energy gaps, creating an energetic barrier that inhibits charge transfer between crystalline and disordered domains. This heterogeneity in energy landscape and molecular order within P3HT films imposes a significant limitation on charge transport.[47] In thin P3HT films, the crystalline domains, composed of networks of polymer main chains with π–π stacking, can exhibit different orientations relative to the substrate. Depending on the preparation conditions, the crystalline domains of P3HT can adopt face-on or edge-on orientations. In the face-on orientation, the thiophene rings are oriented

Table 2 Melting and crystallization temperatures measured by BDS

Sample name	T_m (°C)	T_c (°C)
Bulk	232	209, 220
Nanowire	229	190, 198
NT1	229	208, 224
NT2	223	207, 222
NT3	222	205, 221
NT4	219	203, 220
NT5	219	203, 217

facing the substrate, positioning the *a* and *c* axes within the substrate plane. Conversely, in the edge-on orientation, the direction of π-stacking lies in the plane, placing the *b* and *c* axes in the substrate plane. Depending on the preparation method, both orientations can coexist or one orientation can be dominant in thin films. Deepak Gargi *et al.* demonstrated for instance that charge transport mechanisms within P3HT films oriented in the "face-on" configuration were more efficient.[18] In the case of nanowires, the crystalline structure was analyzed using X-ray diffraction (XRD) in out-of-plane configuration (X-ray beam perpendicular to the nanopore axis) and in-plane (X-ray beam parallel to the nanopore axis). Jaime Martín *et al.*[15] demonstrated that confinement significantly altered the molecular arrangement of P3HT nanowires. For nanowires confined within 250 nm nanopores, the π–π stacking direction was predominantly aligned parallel to the nanopore axis (or perpendicular to the AAO pore walls), enhancing the material's optoelectronic properties. However, as the degree of confinement increased, a change in orientation was observed. In nanopores with diameters smaller than 60 nm, the π–π stacking direction became perpendicular to the nanopore axis. This finding illustrates that reducing the degree of confinement (*i.e.*, reducing the nanopore diameter) can control the polymer chain orientation by increasing the surface-to-volume ratio between the polymer and AAO walls. For nanotubes formed in 200 nm nanopores, a similar orientation was observed:[17] the π–π stacking direction aligned along the nanopore axis, resulting in a tenfold increase in the electrical conductivity of P3HT nanotubes.[14] In the out-of-plane configuration, the presence of the (020) plane confirmed that the π–π stacking direction was parallel to the nanotube's long axis, indicating a *b*-axis orientation of P3HT crystals.[52] In the in-plane configuration, a strong (100) Bragg reflection demonstrated that the *a*-axis was oriented perpendicularly to the nanotube's long axis.[52]

To compare the crystalline structure of P3HT in the bulk, nanowires, and nanotubes, WAXS measurements were performed in the present study (Fig. 5). The P3HT in the bulk exhibits several characteristic Bragg peaks, with no preferential orientation. Using Scherrer's equation (eqn (6)) and the full width at half maximum (FWHM) of the (100) peak observed at $q = 0.38 \text{ Å}^{-1}$, the crystal size perpendicular to the (100) planes was calculated to be approximately 11 nm.

Fig. 5 (lower part) presents as well WAXS results for P3HT nanowires and nanotubes measured in the out-of-plane configuration within AAO membranes. To isolate the crystalline response of P3HT, the membrane signals were subtracted (SI, Fig. S7). The diffraction pattern of P3HT nanowires was dominated by the (100) reflection, while the (020) reflection was significantly reduced compared to bulk P3HT, indicating a clear preferential alignment of polymer crystals along the nanopore axis. The scattering diagrams for P3HT nanotubes displayed a similar pattern, with a pronounced (100) reflection, confirming that the crystalline structure was aligned along the nanopore axis, as also observed in the nanowire configuration. Notably, the (100) peak intensity was strongly influenced by nanotube thickness: thinner nanotubes exhibited lower intensities, indicating reduced crystallinity. This orientation effect,
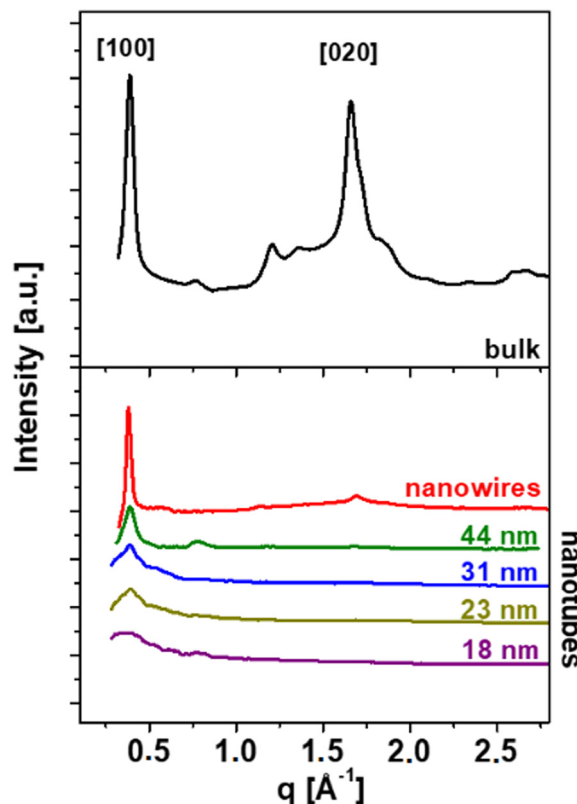

Fig. 5 X-Ray diffraction diagrams for bulk P3HT, nanowires and nanotubes of different thicknesses, as indicated. The contribution of the empty AAO were subtracted from the signal, and the nanopores axis were parallel to incident beam. The energy of the photon beam was 18 keV.

previously observed in both P3HT nanowires and nanotubes, supports the enhancement in the conductivity of P3HT nanowires and nanotubes as compared to the conductive properties of the bulk P3HT which lacks preferential orientation. The P3HT nanotubes with a 44 nm thickness exhibit a higher conductivity than the P3HT nanowires. This improved performance can be attributed to the more effective orientation of the π–π stacking in nanotubes. The (020) reflection observed in
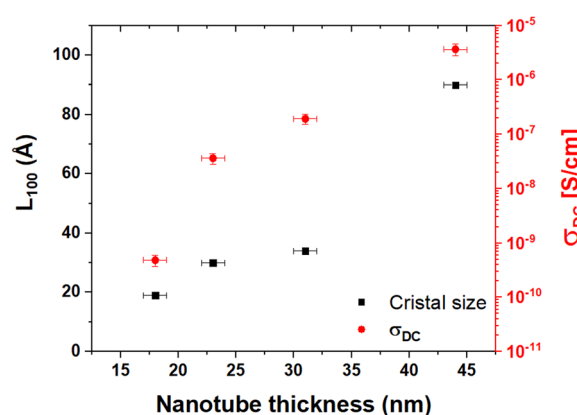

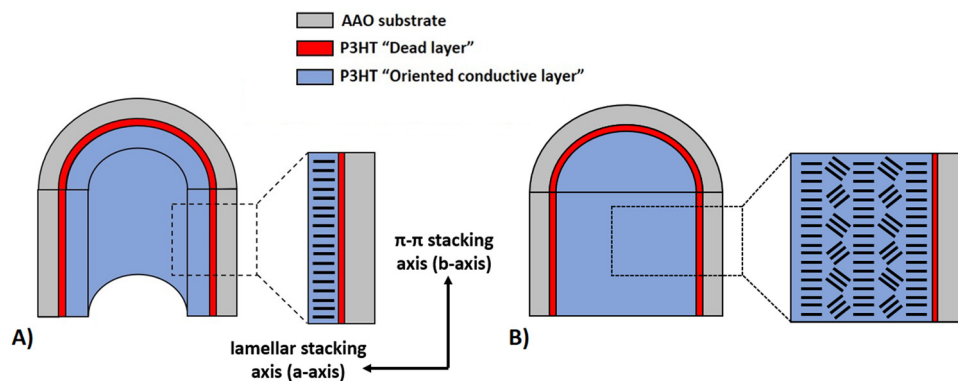Fig. 6 Crystal size and conductivity of P3HT nanotubes as a function of nanotube thickness.

Fig. 7 Schematic representation of the cross-section of a nanopore containing P3HT nanotubes (A) and nanowires (B) showing the interplay between orientation effects and interfacial interactions. These effects lead to changes by order of magnitude in the conductivity value of P3HT nanotubes.

nanowires suggests that a portion of polymer chains may be misaligned, causing slight conductivity losses not present in 44 nm nanotubes. The reason for the more ordered state observed in the nanotubes is related to the fact that, in nanotubes, the chains configuration is completely governed by surface effects, while in nanowires, additional contributions are superposing, especially from the middle of the nanopores where surface effects are becoming less effective.

The reduced intensity of the (100) peak with decreasing nanotube thickness indicates a loss of crystallinity. While the precise degree of crystallinity is challenging to determine, the crystal size can be estimated using the Scherrer equation:

$$L_{100} \approx \frac{2\pi}{\Delta q} \qquad (6)$$

where L_{100} represents the crystal size perpendicular to the (100) planes and Δq the full width at half maximum of the (100) peak.

Fig. 6 illustrates the relationship between crystal size, conductivity, and nanotube thickness. As expected, crystal size decreases with thinner nanotubes, accompanied by a corresponding drop in conductivity. This correlation length, corresponding to the long axis of the nanopores, highlights the influence of crystallinity on the electrical performance.

These crystallization effects are similar to those observed in thin films, where a decrease in film thickness reduces crystallinity and consequently conductivity.[25] In thinner nanotubes, surface-induced effects, including diminished crystallinity and increased polymer chain adsorption at the walls, result in significant conductivity losses. Conversely, in thicker nanotubes, orientation effects predominate, enhancing conductivity to levels surpassing bulk P3HT and P3HT nanowires. This behavior, observed in 44 nm nanotubes, underscores the interplay between surface and orientation effects in confined geometries, as schematically illustrated in Fig. 7.

The competition between different overlapping phenomena taking place at the nanoscale can be thus effectively used as a powerful tool to modulate – over many orders of magnitude – the conductive properties of conjugated polymers and give rise to new nanomaterials exhibiting better properties than in the

bulk. This could have potential applications in numerous fields using functional nanomaterials with enhanced performance.

4. Conclusions

In this work, a comprehensive comparison of the conductive properties of P3HT has been carried-out in three different states: bulk, nanowires and nanotubes. This approach has been combined with a systematic variation of the nanotubes thickness, with the goal of assessing different mechanisms taking place at the nanoscale and impacting the conductive properties of the polymer. It was found that the conductivity value of nanotubes strongly depends on the nanotubes thickness, with variations by 5 orders of magnitude being measured. At lower nanotube thicknesses, surface-induced effects, manifested by a slowing-down of the charge carrier mobility and a decrease in the crystals size, are playing the dominant role, leading to a pronounced decrease in conductivity. These effects, detrimental to the conductive properties of P3HT, are overrun by orientation effect of the polymer chains at larger nanotubes thicknesses, leading to conductivity values that are higher than the conductivity of the bulk. A noticeable difference in conductivity is found between nanowires and nanotubes, the latter being more conductive than the former, while both are more conductive than the bulk. The origin of the enhancement effect is related to the crystalline structure that is that is oriented in the nanopores by positioning the π–π stacking parallel to the nanopores axis. Nanoconfinement and the wealth of different overlapping phenomena taking place at the nanoscale could represent thus a powerful tool to broadly modulate the conductive properties of conjugated polymers and give rise to nanomaterials exhibiting better properties than in the bulk.

Conflicts of interest

There are no conflicts to declare.

Data availability

The data that support the findings of this study are available from the corresponding author upon reasonable request. All

relevant data generated or analysed during this study have been included in this published article and its SI. Where applicable, datasets have been deposited in publicly accessible repositories, with links and identifiers provided in the article.

Supplementary information containing additional schemas and experimental data on samples preparation and characterization is available. See DOI: https://doi.org/10.1039/d5sm00507h

Acknowledgements

References

1 J. S. Kim, et al., Poly(3-hexylthiophene) nanorods with aligned chain orientation for organic photovoltaics, Adv. Funct. Mater., 2010, 20(4), 540–545, DOI: 10.1002/adfm.200901760.

2 M. Aryal, K. Trivedi and W. Hu, Nano-confinement induced chain alignment in ordered P3HT nanostructures defined by nanoimprint lithography, ACS Nano, 2009, 3(10), 3085–3090, DOI: 10.1021/nn900831m.

3 J. Zaumseil, P3HT and other Polythiophene field-effect transistors, Adv. Polym. Sci., 2014, 265, 107–138, DOI: 10.1007/12_2014_279.

4 U. Bielecka, P. Lutsyk, K. Janus, J. Sworakowski and W. Bartkowiak, Effect of solution aging on morphology and electrical characteristics of regioregular P3HT FETs fabricated by spin coating and spray coating, Org. Electron., 2011, 12(11), 1768–1776, DOI: 10.1016/j.orgel.2011.06.027.

5 D. Chen, W. Zhao and T. P. Russell, P3HT nanopillars for organic photovoltaic devices nanoimprinted by AAO templates, ACS Nano, 2012, 6(2), 1479–1485, DOI: 10.1021/nn2043548.

6 M. M. Rojo, J. Martín, S. Grauby, T. Borca-Tasciuc, S. Dilhaire and M. Martin-Gonzalez, Decrease in thermal conductivity in polymeric P3HT nanowires by size-reduction induced by crystal orientation: New approaches towards thermal transport engineering of organic materials, Nanoscale, 2014, 6(14), 7858–7865, DOI: 10.1039/c4nr00107a.

7 J. P. Cannon, S. D. Bearden and S. A. Gold, Effect of wetting solvent on poly(3-hexylthiophene) (P3HT) nanotubles fabricated via template wetting, Synth. Met., 2010, 160(23–24), 2623–2627, DOI: 10.1016/J.SYNTHMET.2010.10.014.

8 S. Baek, J. B. Park, W. Lee, S. H. Han, J. Lee and S. H. Lee, A facile method to prepare regioregular poly(3-hexylthiophene) nanorod arrays using anodic aluminium oxide templates and capillary force, New J. Chem., 2009, 33(5), 986–990, DOI: 10.1039/b821288k.

9 S. Liu, J. Tian and W. Zhang, Fabrication and application of nanoporous anodic aluminum oxide: A review, Nanotechnology, 2021, 32, 222001, DOI: 10.1088/1361-6528/abe25f.

10 S. Manzoor, M. W. Ashraf, S. Tayyaba, M. I. Tariq and M. K. Hossain, Recent Progress of Fabrication, Characterization, and Applications of Anodic Aluminum Oxide (AAO) Membrane: A Review, Comput. Model. Eng. Sci., 2023, 135(2), 1007–1052, DOI: 10.32604/cmes.2022.022093.

11 X. Huang, H. Mutlu, W. Dong and P. Theato, Polymeric Janus nanorods via anodic aluminum oxide templating, Soft Matter, 2023, 19(30), 5663–5667, DOI: 10.1039/d3sm00751k.

12 C. H. Woo, C. Piliego, T. W. Holcombe, M. F. Toney and J. M. J. Fréchet, A quantitative correlation between the mobility and crystallinity of photo-cross-linkable P3HT, Macromolecules, 2012, 45(7), 3057–3062, DOI: 10.1021/ma202203z.

13 I. Roy and S. Hazra, Solvent dependent ordering of poly(3-dodecylthiophene) in thin films, Soft Matter, 2015, 11(18), 3724–3732, DOI: 10.1039/c5sm00595g.

14 J. Byun, Y. Kim, G. Jeon and J. K. Kim, Ultrahigh density array of free-standing poly(3-hexylthiophene) nanotubes on conducting substrates via solution wetting, Macromolecules, 2011, 44(21), 8558–8562, DOI: 10.1021/ma202018m.

15 J. Martín, et al., Poly(3-hexylthiophene) nanowires in porous alumina: Internal structure under confinement, Soft Matter, 2014, 10(18), 3335–3346, DOI: 10.1039/c3sm52378k.

16 D. Pourjafari, T. Serrano, B. Kharissov, Y. Peña and I. Gómez, Template assisted synthesis of poly(3-hexylthiophene) nanorods and nanotubes: Growth mechanism and corresponding band gap, Int. J. Mater. Res., 2015, 106(4), 414–420, DOI: 10.3139/146.111196.

17 L. H. Jimison, S. Himmelberger, D. T. Duong, J. Rivnay, M. F. Toney and A. Salleo, Vertical confinement and interface effects on the microstructure and charge transport of P3HT thin films, J. Polym. Sci., Part B:Polym. Phys., 2013, 51(7), 611–620, DOI: 10.1002/polb.23265.

18 D. Gargi, R. J. Kline, D. M. Delongchamp, D. A. Fischer, M. F. Toney and B. T. O'Connor, Charge transport in highly face-On Poly(3-hexylthiophene) films, J. Phys. Chem. C, 2013, 117(34), 17421–17428, DOI: 10.1021/jp4050644.

19 R. Palacios, et al., Template-assisted fabrication and characterization of photoluminescent polymer nanopillars, Phys. Status Solidi C, 2011, 8(9), 2612–2616, DOI: 10.1002/pssc.201084122.

20 A. P. Holt, et al., Dynamics at the polymer/nanoparticle interface in poly(2-vinylpyridine)/silica nanocomposites, Macromolecules, 2014, 47(5), 1837–1843, DOI: 10.1021/ma5000317.

21 C. R. Snyder, J. S. Henry and D. M. Delongchamp, Effect of regioregularity on the semicrystalline structure of poly(3-hexylthiophene), Macromolecules, 2011, 44(18), 7088–7091, DOI: 10.1021/ma201604n.

22 A. Serghei, D. Chen, D. H. Lee and T. P. Russell, Segmental dynamics of polymers during capillary flow into nanopores, Soft Matter, 2010, 6, 1111–1113.

23 A. Houachtia, P. Alcouffe, G. Boiteux, G. Seytre, J.-F. Gérard and A. Serghei, Nanofluidics Approach to Separate between

Static and Kinetic Nanoconfinement Effects on the Crystallization of Polymers, *Nano Lett.*, 2015, **15**, 4311–4316.

24 G. A. Chahine, N. Blanc, S. Arnaud, F. De Geuser, R. Guinebretière and N. Boudet, Advanced Non-Destructive in Situ Characterization of Metals with the French Collaborating Research Group D2AM/BM02 Beamline at the European Synchrotron Radiation Facility, *Metals*, 2019, **9**(3), 352, DOI: **10.3390/met9030352**.

25 M. K. Smith, V. Singh, K. Kalaitzidou and B. A. Cola, Poly(3-hexylthiophene) nanotube array surfaces with tunable wetting and contact thermal energy transport, *ACS Nano*, 2015, **9**(2), 1080–1088, DOI: **10.1021/nn5027406**.

26 S. Ganguly, S. Sikdar and S. Basu, Experimental investigation of the effective electrical conductivity of aluminum oxide nanofluids, *Powder Technol.*, 2009, **196**(3), 326–330, DOI: **10.1016/j.powtec.2009.08.010**.

27 H. H. Liao, C. M. Yang, C. C. Liu, S. F. Horng, H. F. Meng and J. T. Shy, Dynamics and reversibility of oxygen doping and de-doping for conjugated polymer, *J. Appl. Phys.*, 2008, **103**, 104506, DOI: **10.1063/1.2917419**.

28 J. Obrzut and K. A. Page, Electrical conductivity and relaxation in poly(3-hexylthiophene), *Phys. Rev. B: Condens. Matter Mater. Phys.*, 2009, **80**, 19, DOI: **10.1103/PhysRevB.80.195211**.

29 M. Girtan, On the stability of the electrical and photoelectrical properties of P3HT and P3HT:PCBM blends thin films, *Org. Electron.*, 2013, **14**(1), 200–205, DOI: **10.1016/j.orgel.2012.10.023**.

30 R. Singh, R. K. Singh, J. Kumar, R. Kant and V. Kumar, The origin of DC electrical conduction and dielectric relaxation in pristine and doped poly 3-hexylthiophene films, *J. Polym. Sci., Part B:Polym. Phys.*, 2010, **48**(10), 1047–1053, DOI: **10.1002/polb.21994**.

31 S. Ukai, H. Ito, K. Marumoto and S. I. Kuroda, Electrical conduction of regioregular and regiorandom poly(3-hexylthiophene) doped with iodine, *J. Phys. Soc. Jpn.*, 2005, **74**(12), 3314–3319, DOI: **10.1143/JPSJ.74.3314**.

32 D. Richter and M. Kruteva, Polymer dynamics under confinement, *Soft Matter*, 2019, DOI: **10.1039/c9sm01141b**.

33 C. Tsonos, A. Kanapitsas, A. Kechriniotis and N. Petropoulos, AC and DC conductivity correlation: The coefficient of Barton-Nakajima-Namikawa relation, *J. Non-Cryst. Solids*, 2012, **358**(14), 1638–1643, DOI: **10.1016/j.jnoncrysol.2012.04.029**.

34 L. Janasz, *et al.*, Improved charge carrier transport in ultrathin poly(3-hexylthiophene) films *via* solution aggregation, *J. Mater. Chem. C*, 2016, **4**(48), 11488–11498, DOI: **10.1039/c6tc02142e**.

35 L. Janasz, *et al.*, Microstructure-Dependent Charge Carrier Transport of Poly(3-hexylthiophene) Ultrathin Films with Different Thicknesses, *Langmuir*, 2017, **33**(17), 4189–4197, DOI: **10.1021/acs.langmuir.7b00563**.

36 A. Serghei, J. L. Lutkenhaus, D. F. Miranda, K. McEnnis, F. Kremer and T. P. Russell, Density Fluctuations and Phase Transitions of Ferroelectric Polymer Nanowires, *Small*, 2010, **6**, 1822–1826, DOI: **10.1002/smll.201000562**.

37 A. Serghei, W. Zhao, D. Miranda and T. P. Russell, Curie transitions for attograms of ferroelectric polymers, *Nano Lett.*, 2013, **13**(2), 577–580, DOI: **10.1021/nl304103y**.

38 Q. Jiang, C. C. Yang and J. C. Li, *Size-Dependent Melting Temperature of Polymers*.

39 J. H. Kim, J. Jang and W.-C. Zin, *Thickness Dependence of the Melting Temperature of Thin Polymer Films*.

40 D. Dudenko, *et al.*, A Strategy for Revealing the Packing in Semicrystalline π-Conjugated Polymers: Crystal Structure of Bulk Poly-3-hexyl-thiophene (P3HT), *Angew. Chem.*, 2012, **124**(44), 11230–11234, DOI: **10.1002/ange.201205075**.

41 J. Balko, R. H. Lohwasser, M. Sommer, M. Thelakkat and T. Thurn-Albrecht, Determination of the crystallinity of semicrystalline poly(3-hexylthiophene) by means of wide-angle X-ray scattering, *Macromolecules*, 2013, **46**(24), 9642–9651, DOI: **10.1021/ma401946w**.

42 X. Shen, W. Hu and T. P. Russell, Measuring the degree of crystallinity in semicrystalline regioregular poly(3-hexylthiophene), *Macromolecules*, 2016, **49**(12), 4501–4509, DOI: **10.1021/acs.macromol.6b00799**.

43 B. Kuei and E. D. Gomez, Chain conformations and phase behavior of conjugated polymers, *Soft Matter*, 2017, DOI: **10.1039/C6SM00979D**.

44 A. D. Printz and D. J. Lipomi, *Competition between deformability and charge transport in semiconducting polymers for flexible and stretchable electronics*, 2016, American Institute of Physics Inc., DOI: **10.1063/1.4947428**.

45 S. Giannini and J. Blumberger, *Charge Transport in Organic Semiconductors: The Perspective from Nonadiabatic Molecular Dynamics*, 2022, American Chemical Society. , DOI: **10.1021/acs.accounts.1c00675**.

46 M. Brinkmann, *Structure and morphology control in thin films of regioregular poly(3-hexylthiophene)*, 2011, DOI: **10.1002/polb.22310**.

47 R. Noriega, *et al.*, A general relationship between disorder, aggregation and charge transport in conjugated polymers, *Nat. Mater.*, 2013, **12**(11), 1038–1044, DOI: **10.1038/nmat3722**.

48 A. Salleo, R. J. Kline, D. M. DeLongchamp and M. L. Chabinyc, Microstructural characterization and charge transport in thin films of conjugated polymers, *Adv. Mater.*, 2010, **22**(34), 3812–3838, DOI: **10.1002/adma.200903712**.

49 S. A. Mollinger, B. A. Krajina, R. Noriega, A. Salleo and A. J. Spakowitz, Percolation, Tie-Molecules, and the Microstructural Determinants of Charge Transport in Semicrystalline Conjugated Polymers, *ACS Macro Lett.*, 2015, **4**(7), 708–712, DOI: **10.1021/acsmacrolett.5b00314**.

50 F. C. Spano, Modeling disorder in polymer aggregates: The optical spectroscopy of regioregular poly(3-hexylthiophene) thin films, *J. Chem. Phys.*, 2005, **122**, 234701, DOI: **10.1063/1.1914768**.

51 A. Troisi, The speed limit for sequential charge hopping in molecular materials, *Org. Electron.*, 2011, **12**(12), 1988–1991, DOI: **10.1016/j.orgel.2011.08.020**.

52 W. Xiang, X. Sun, Z. Ren, J. Zhang, H. Li and S. Yan, Diameter and thermal treatment dependent structure and optical properties of poly(3-hexylthiophene) nanotubes, *J. Mater. Chem. C*, 2017, **5**(32), 8315–8322, DOI: **10.1039/c7tc00947j**.